

# A Bayesian framework for infrasound location

Ryan T. Modrak, Stephen J. Arrowsmith and Dale N. Anderson

Los Alamos National Laboratory, EES-17, Los Alamos, NM, USA. E-mail: sarrowsmith@gmail.com

Accepted 2009 December 23. Received 2009 December 18; in original form 2009 August 20

## SUMMARY

We develop a framework for location of infrasound events using backazimuth and infrasonic arrival times from multiple arrays. Bayesian infrasonic source location (BISL) developed here estimates event location and associated credibility regions. BISL accounts for unknown source-to-array path or phase by formulating infrasonic group velocity as random. Differences between observed and predicted source-to-array traveltimes are partitioned into two additive Gaussian sources, measurement error and model error, the second of which accounts for the unknown influence of wind and temperature on path. By applying the technique to both synthetic tests and ground-truth events, we highlight the complementary nature of back azimuths and arrival times for estimating well-constrained event locations. BISL is an extension to methods developed earlier by Arrowsmith *et al.* that provided simple bounds on location using a grid-search technique.

**Key words:** Probability distributions; Seismic monitoring and test-ban treaty verification; Statistical seismology.

## INTRODUCTION

### Background

Low frequency acoustic waves propagate large distances through the Earth's atmosphere and, represented mathematically, provide a means of locating explosions, earthquakes, and other events. Infrasound monitoring networks have existed for several decades but development of location capabilities has progressed relatively slowly, largely as a consequence of two factors. First, the location problem is complicated by the effects of spatially and temporally variable winds and temperatures. These parameters exert a strong influence on infrasound propagation (Garces *et al.* 1998) and vary over relatively short times and distances (Drob 2004). Current models of atmospheric winds and temperatures do not capture sufficient temporal or spatial resolution to reliably predict observed infrasonic phases (e.g. Arrowsmith *et al.* 2007). As a result, we contend that a deterministic approach in which we assume *a priori* knowledge of the medium properties is not currently feasible for operational processing. [In a promising step toward this goal, detailed studies of ground-truth events have employed variants on Geiger's method with some success, e.g. Evers *et al.* (2007), Ceranna *et al.* (2009). This approach, however, does not yet fully characterize the model uncertainty.]

In addition to the complexities involved with infrasound propagation, a second source of difficulty concerns network coverage. Although the size and sensitivity of infrasound deployments has increased in recent years, infrasound signal analysis is still typically done with sparse configurations, often consisting of only two or three arrays.

Despite these problems, infrasound data provide a powerful means of supplementing observations from seismology and other

technologies. Infrasound sensors are almost always configured in arrays, providing backazimuths and horizontal velocity components in addition to amplitudes and arrival times. A strength of infrasound analysis is the reliability of these backazimuth estimates, which are obtained from slight differences in arrival times over an array. The reliability of backazimuths is a function of the magnitude of lateral deviations in medium properties, which is significantly less in the atmosphere than in the solid earth.

This paper addresses the need for a robust infrasound location algorithm that does not require *a priori* knowledge of atmospheric properties—although such information can be incorporated where available—but allows for computation of source likelihood regions based on statistical assumptions about the data. Bayesian infrasonic source location (BISL) exploits the unique advantages of infrasound signals (accurate backazimuths and arrival times) while accounting for the disadvantages (uncertainty of medium characteristics).

### Automatic detection and location algorithms

The use of infrasound in both applied and scientific contexts has spurred the creation of new regional networks (e.g. Stump *et al.* 2004). Partly in response to these new deployments, algorithms for the automatic detection and location of infrasound sources have been proposed by Le Pichon *et al.* (2008) and Arrowsmith *et al.* (2008). Both studies demonstrate detection and location capabilities using ground-truth events—Le Pichon *et al.* (2008) for a collection of events in Central Europe, and Arrowsmith *et al.* (2008) for one in the Western United States.

While both studies display a high level of success in these experiments, the methodologies employed in each case are quite different. Le Pichon *et al.* (2008) formulate the problem as a system of

equations solved using a constant atmospheric velocity model and a least squares approach. An initial solution for use in the inversion is obtained from backazimuth data and refined through successive iterations. In contrast, Arrowsmith *et al.* (2008) use a grid search procedure to determine a preliminary source region rather than a single estimated source location. Once a set of arrivals has been recognized as an event, boundaries for the source region are obtained by assuming fixed bounds on the group velocity (or celerity) of the infrasound signal and on the error in the observed backazimuths.

Building on the work of Arrowsmith *et al.* (2008), the BISL algorithm developed here combines the likelihood equations for backazimuth and traveltimes constraints to assign a combined likelihood value to the location parameters. The prior probability density function (prior PDF) for velocity serves to account for unknown path and phase. Integration across group velocity yields the marginal posterior probability density function (marginal posterior PDF), from which Bayesian credibility contours for source location are determined. These contours need not be—but given Gaussian statistical assumptions, often are—ellipsoidal. Fagan *et al.* (2009) propose a similar framework for single event location from seismic first arrivals.

## METHOD

The data used in this study consist of backazimuth and arrival time vectors

$$\theta = [\theta_1, \dots, \theta_n], \quad \mathbf{t} = [t_1, \dots, t_n],$$

in which the subscript denotes the array at which the observation was recorded. Following the same subscript convention, the coordinates of the  $i$ th array are represented by  $x_i$  and  $y_i$ . For simplicity, we outline the equations below using Cartesian coordinates, although we apply the technique to the ground-truth examples using spherical coordinates.

As discussed by Garces *et al.* (2002), horizontal slowness, or equivalently, phase velocity, does not lead to unambiguous phase identification without accurate knowledge of atmospheric winds. Because our methodology is designed to be applicable without knowledge of atmospheric winds, this constraint is not used in the location algorithm.

To estimate origin time and source location, we search over a uniformly spaced grid in  $t$ ,  $x$ ,  $y$  and  $v$  for the most likely time, location and group velocity, respectively. A candidate origin time is represented by  $t_0$ , a candidate source location by  $x_0$  and  $y_0$ , and a candidate group velocity by  $v$ . Here, we treat  $v$  as an independent parameter which can be removed later by integration. This approach greatly simplifies the formulation of the likelihood function, enabling straightforward comparison between the observed and predicted arrival times.

Using the notation  $\mathbf{d} \equiv \{\mathbf{t}, \theta\}$  and  $\mathbf{m} \equiv \{t_0, x_0, y_0, v\}$ , the posterior probability density function (posterior PDF) is

$$P(\mathbf{m}|\mathbf{d}) = c(\mathbf{d})P(\mathbf{m})P(\mathbf{d}|\mathbf{m}), \quad (1)$$

where  $P(\mathbf{m})$  is the prior PDF for the model parameters,  $P(\mathbf{d}|\mathbf{m})$  is the likelihood function that would generate data  $\mathbf{d}$  given fixed model parameters  $\mathbf{m}$ , and  $c(\mathbf{d})$  ensures that  $P(\mathbf{m}|\mathbf{d})$  integrates to unity.

### Prior PDF

Applying eq. (1) requires distinguishing between *a priori* information and data; the former are incorporated in the prior PDF and

the latter are incorporated in the likelihood function. To constrain unknown group velocity between source and receiver, we define the prior PDF on  $v$  to be

$$p(v) \equiv \begin{cases} 16.67 & 0.28 \text{ km s}^{-1} \leq v \leq 0.34 \text{ km s}^{-1} \\ 0 & \text{otherwise} \end{cases}, \quad (2)$$

where the bounds 0.28 and 0.34 km s<sup>-1</sup> are modified from Cepplecha *et al.* (1998) to the case of high-frequency arrivals recorded on a regional network (i.e. direct infrasonic surface waves through stratospheric returns). The value 16.67 is chosen so that  $p(v)$  integrates to unity. In this formulation, the priors on  $t_0$ ,  $x_0$  and  $y_0$  are independent over physically reasonable ranges so that to a first approximation

$$P(\mathbf{m}) = p(v)p(t_0)p(x_0, y_0). \quad (3)$$

Although eq. (2) comprises a uniform distribution, the technique readily accommodates a more physically constraining prior PDF on  $v$ . Even so, the use of a single group velocity parameter—as opposed to one parameter for each array—requires that the same value  $v$  be used to compute the predicted arrival times at all arrays. The likelihood function will, as a result, favour parameter combinations in which the predicted group velocities at each array are similar. This drawback is addressed by folding group velocity uncertainty into a model error term, described below. In general the method is better suited for regional networks, such as those in the ground truth examples discussed below, than it is for global networks where phase and group velocities might vary less predictably.

### Likelihood function

The likelihood function is a product of backazimuth and arrival time components over all arrays:

$$P(\mathbf{d}|\mathbf{m}) \equiv \prod_{i=1}^n \Theta_i(\theta_i|\mathbf{m})\Phi_i(t_i|\mathbf{m}). \quad (4)$$

For a given station  $i$ , the component  $\Theta_i$  measures how well the observed backazimuth agrees with the chosen model parameters. More specifically,  $\Theta_i$  gives the likelihood of observing  $\theta_i$  assuming known statistical distribution of errors and assuming the current choice of model parameters  $\mathbf{m}$  is the correct one. The likelihood component  $\Phi_i$  measures the agreement between the observed and the predicted arrival times under similar assumptions.

Assuming Gaussian distributed errors, the backazimuth likelihood component is

$$\Theta_i(\theta_i|\mathbf{m}) \equiv \frac{1}{\sqrt{2\pi\sigma_\theta^2}} \exp\left[-\frac{1}{2}\left(\frac{\gamma_i}{\sigma_\theta}\right)^2\right] \quad (5)$$

and the arrival time likelihood component is

$$\Phi_i(t_i|\mathbf{m}) \equiv \frac{1}{\sqrt{2\pi\sigma_\phi^2}} \exp\left[-\frac{1}{2}\left(\frac{\epsilon_i}{\sigma_\phi}\right)^2\right]. \quad (6)$$

With  $d_i = d_i(x_0, y_0, x_i, y_i)$  as the distance from the candidate source to the  $i$ th array, the residuals are

$$\gamma_i \equiv \theta_i - \arctan\left(\frac{y_i - y_0}{x_i - x_0}\right), \quad (7)$$

$$\epsilon_i \equiv t_i - \left(t_0 + \frac{d_i}{v}\right). \quad (8)$$

The total variances in the backazimuths and arrival times (accounting for both measurement and model error contributions, see next section) are denoted  $\sigma_\theta^2$  and  $\sigma_\phi^2$ , respectively.

### Marginal posterior PDF

The marginal posterior PDF is obtained by numerically integrating the posterior PDF in eq. (1) across group velocity  $v$ . Computing the marginal posterior PDF enables estimation of origin time and source location. To plot the results using a 2-D set of axes it is often useful to integrate across origin time  $t$  as well. We use this technique, along with a uniform grid in  $x$  and  $y$ , to generate figures for the synthetic and ground-truth events below.

Having computed the marginal posterior PDF, we wish to estimate the origin time and source location and determine credibility contours around them. With zero-one loss, the Bayesian estimate of source location and origin time is the mode of the marginal posterior PDF (Bernardo & Smith 2000; Berger 1985). In our development we use zero-one loss; that is, we select posterior mode values as estimates of source location and origin time. To determine credibility contours, we take fixed slices through the marginal posterior PDF, defining sets in  $\{t, x, y\}$ . Integrating over these sets yields Bayesian credibility values from which contours are drawn.

### Representation of error

Differences between observed and predicted values of  $\theta_i$  and  $t_i$  are assumed to arise from two uncorrelated, additive sources—measurement error and model error. Once variances have been determined for both, the terms combine as follows to give the total variances used in eqs (5) and (6):

$$\sigma_{\theta}^2 = \sigma_{\theta,\text{meas}}^2 + \sigma_{\theta,\text{mod}}^2, \quad \sigma_{\phi}^2 = \sigma_{\phi,\text{meas}}^2 + \sigma_{\phi,\text{mod}}^2. \quad (9)$$

In practice,  $\sigma_{\theta}^2$  can be determined empirically using ground-truth events. In particular, an analysis of earthquakes in the Western United States (Mutschlechner & Whitaker 2005) suggests  $\sigma_{\theta} = 3.5^\circ$ . Follow-on work will demonstrate empirical decomposition of  $\sigma_{\theta}^2$  into the variance components  $\sigma_{\theta,\text{meas}}^2$  and  $\sigma_{\theta,\text{mod}}^2$ . The variance on backazimuth measurement error  $\sigma_{\theta,\text{meas}}^2$  is a function of a range of parameters including the array dimensions, sampling frequency, and wavelength. In contrast, the variance on arrival time measurement error  $\sigma_{\theta,\text{mod}}^2$  results from the effects of variable winds and temperatures (Garces *et al.* 1998). Additional sources of error include the plane wave approximation used to calculate the backazimuths and, if present, elevation differences between sources and arrays.

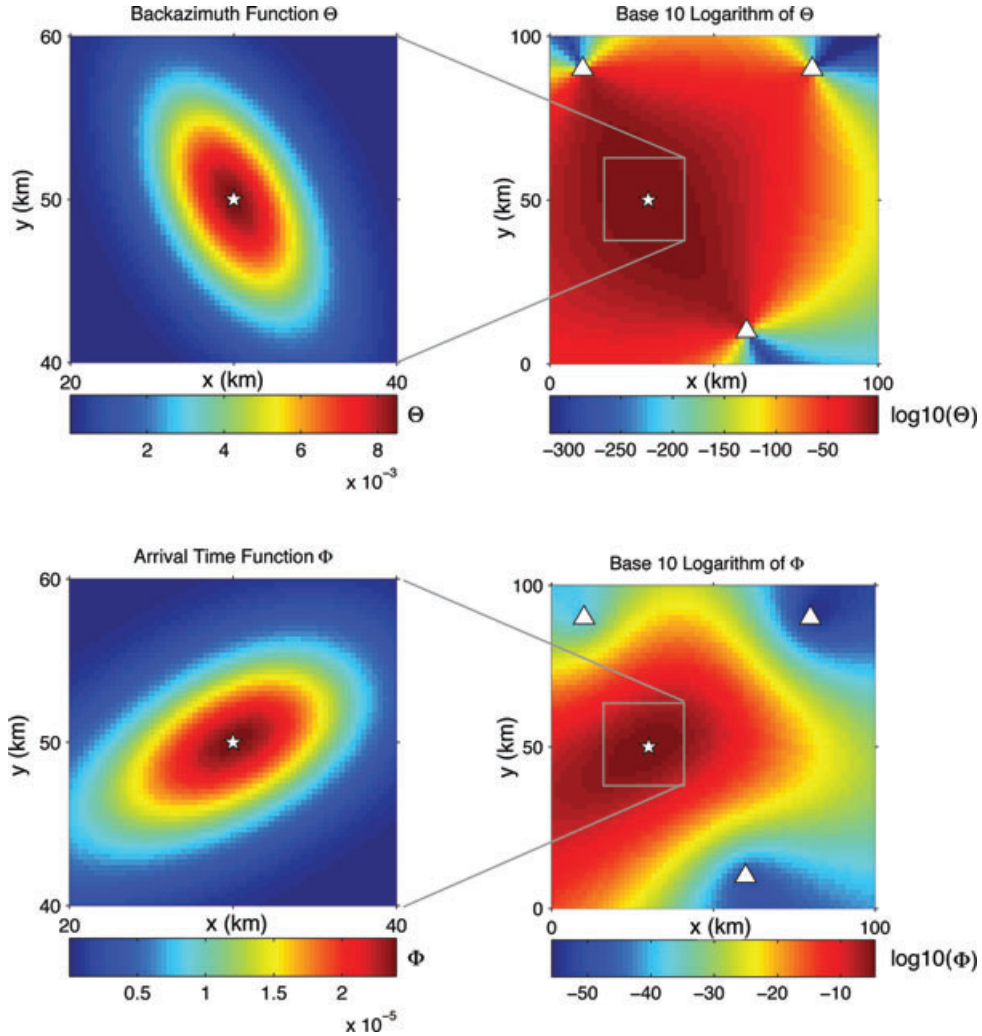


**Figure 1.** Backazimuth  $\Theta$  (top panel) and arrival time  $\Phi$  (bottom panel) likelihood components for a sample synthetic event, obtained by integrating over the parameters  $t$  and  $v$ . The array locations used in computing the likelihood components are marked by triangles. The source location is designated with a star. Note the different spatial scales used to display the likelihood components (on the left-hand side) and their logarithms (on the right-hand side).

Following the rule proposed by Szuberla & Olson (2004), we assume an arrival time measurement error  $\sigma_{\phi, \text{meas}}$  of 0.05 s (for a typical sampling rate of 20 Hz). Given the difficulty in quantifying the model error on arrival time, an empirical estimate of  $\sigma_{\phi, \text{mod}}$  was not attempted here. Instead,  $\sigma_{\phi, \text{mod}}$  was assigned based on the scale of the network configuration—specifically, by assuming a linear relationship between network scale and arrival time model error standard deviation. Though subjective, this approach was found to provide a consistent weighting between the backazimuth and arrival time likelihood components (measured by the magnitude range of these components).

## RESULTS

To illustrate the performance of the algorithm, we present results obtained using a synthetic event and two ground-truth events. The synthetic example shows the algorithm's performance under ideal conditions—with no data errors and with the same group velocity observed at all arrays. The ground-truth examples, in contrast, illustrate performance using backazimuths and arrival times observed at real infrasound arrays.

A simple synthetic configuration consisting of three infrasound arrays and an infrasound source is shown in Figs 1 and 2. For

a suite of source locations, we fix the origin time at  $t = 0$  and assume a constant group velocity  $v = 0.31 \text{ km s}^{-1}$  at all arrays. From these assumptions, synthetic arrival times and backazimuths were computed for each array; no noise was introduced to these synthetic data.

From eq. (4), the likelihood function is composed of factors

$$\Theta(\theta|\mathbf{m}) = \prod_{i=1}^n \Theta_i(\theta_i|\mathbf{m}), \quad \Phi(\mathbf{t}|\mathbf{m}) = \prod_{i=1}^n \Phi_i(t_i|\mathbf{m}). \quad (10)$$

Fig. 1 shows plots of  $\Theta$  and  $\Phi$  for a typical event. The product of these components is proportional, by a constant function of the data, to the posterior PDF. For the simulated event in Fig. 1, this normalizing constant was determined giving the posterior PDF shown in Figs 2(a) and (b). Figs 2(c) and (d), on the other hand, illustrate the construction of Bayesian credibility contours for the sample synthetic event.

We further test BISL using data from a rocket motor explosion at the Utah Test and Training Range (UTTR), recorded at three nearby infrasound arrays (described in Stump *et al.* 2008). For the UTTR event, source location and origin time are known (Table 1). Calculated backazimuths and analyst-determined arrival times are listed in Table 2. The group velocities of infrasonic phases are consistent with direct infrasonic surface waves at all arrays ( $v = 0.35 \text{ km s}^{-1}$

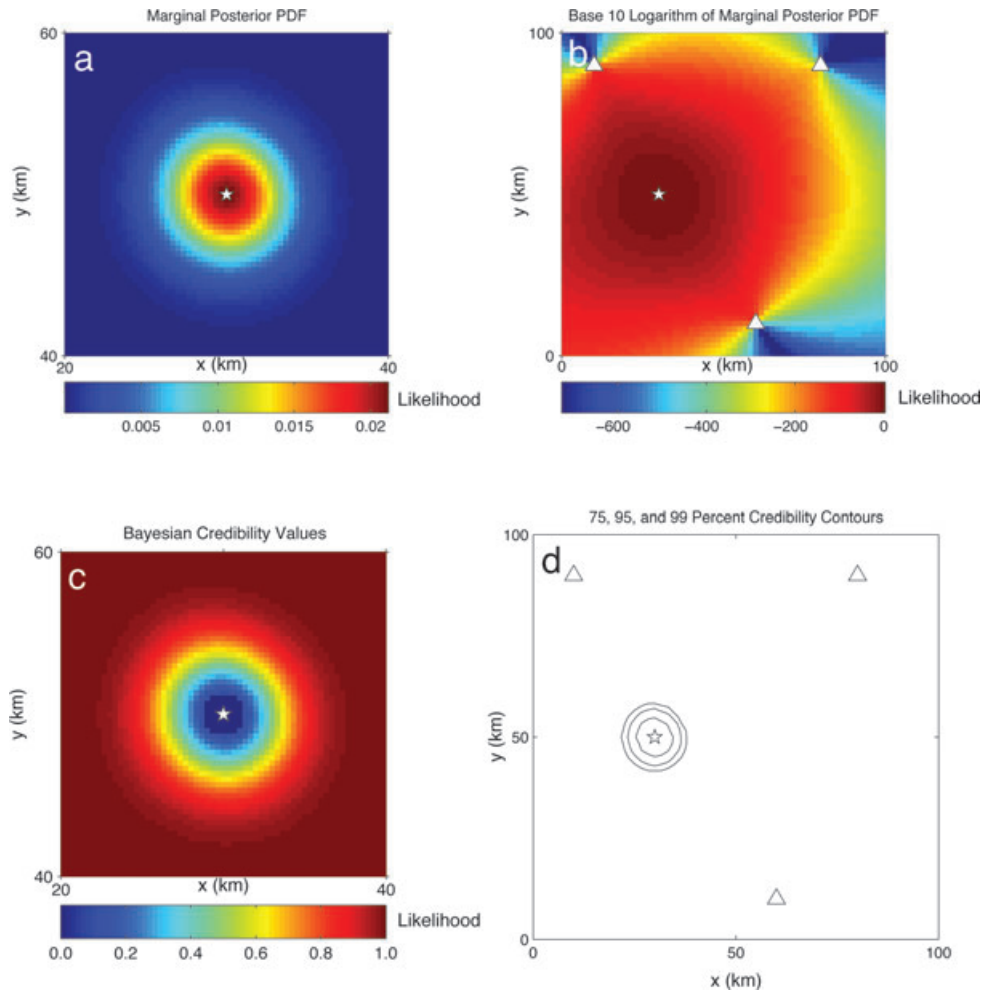


**Figure 2.** Panels (a) and (b) show the marginal posterior PDF for the sample synthetic event, obtained by integrating the posterior PDF over the parameters  $t$  and  $v$ . Panels (c) and (d) show the Bayesian credibility values and associated credibility contours, computed from the values in top panels using the procedure described in the text. Note the differences in axis limits among the panels.

**Table 1.** UTTR ground-truth information.

Source location	41.131, -112.895
Source origin time	20:43:12 2007/08/27

**Table 2.** UTTR observations.

Station	Location	Arrival time	Backazimuth
BGU	40.920, -133.031	20:44:27	30.96
EPU	41.390, -112.410	20:45:35	237.8
NOQ	40.653, -112.119	20:47:17	304.22

at BGU,  $0.35 \text{ km s}^{-1}$  at EPU, and  $0.34 \text{ km s}^{-1}$  at NOQ). Calculations were performed using a spherical coordinate system, though apart from this enhancement, the UTTR event analysis is analogous to that demonstrated with the synthetic example. Figs 3(a) and (b) show the marginal posterior PDF from which Bayesian credibility values are computed and credibility contours drawn (Fig. 3c). The true location is plotted as a star, and the location estimate (posterior mode) is plotted in panel (a) as a rectangle.

The basis of the method outlined in this paper is that, due to uncertainties in atmospheric propagation, we often do not know what phase is being observed at a given array. To address this problem it is useful to assume that the same group velocity value was observed at all arrays (equivalent to assuming the same phase at all arrays). Because this assumption by itself is unrealistic, deviations from the constant group velocity value (or equivalently, uncertainty in phase identification) are folded into the model error term described in eq. (9). To illustrate the performance of the algorithm in the case where we observe different phases at different arrays, we consider the Wells, Nevada earthquake of 2008 February 21 (Arrowsmith

*et al.* 2009). For illustration, we consider arrivals at three arrays (NOQ, NVIAR and PDIAR) for which separation of epicentral and secondary infrasound sources was straightforward (Fig. 4a). The group velocities to each array are  $0.32 \text{ km s}^{-1}$  (NOQ),  $0.31 \text{ km s}^{-1}$  (NVIAR), and  $0.28 \text{ km s}^{-1}$  (PDIAR) suggesting that the arrivals are associated with different propagation paths and phases. Despite this challenge, we obtain a fairly robust location solution using the BISEL method (Fig. 4b) that is consistent with the seismically derived location solution.

**DISCUSSION**

From the results presented above, the algorithm displays at least one prominent similarity with other geophysical location procedures: in all cases, credibility contours generated by the algorithm are strongly ellipsoidal. Only on viewing the logarithm of the posterior likelihood function in Fig. 3 is any pronounced non-ellipsoidal character visible. Because the grid search framework allows for arbitrarily shaped credibility contours, it follows that the statistical assumptions used in formulating the likelihood function (e.g. the use of normally distributed data errors) are responsible for the ellipsoidal contours. Statistical assumptions used in connection with other geophysical locations methods, including covariance matrix analysis in linearized least squares inversions (see Seber & Wild 1989), also produce ellipsoidal uncertainty regions.

Further insight on the shape of the credibility contours can be gained from Fig. 1. For the synthetic configuration shown in the figure, contours of the backazimuth function  $\Theta$  run perpendicular to those of the arrival time function  $\Phi$ , producing nearly circular credibility contours. Though not always as pronounced as in

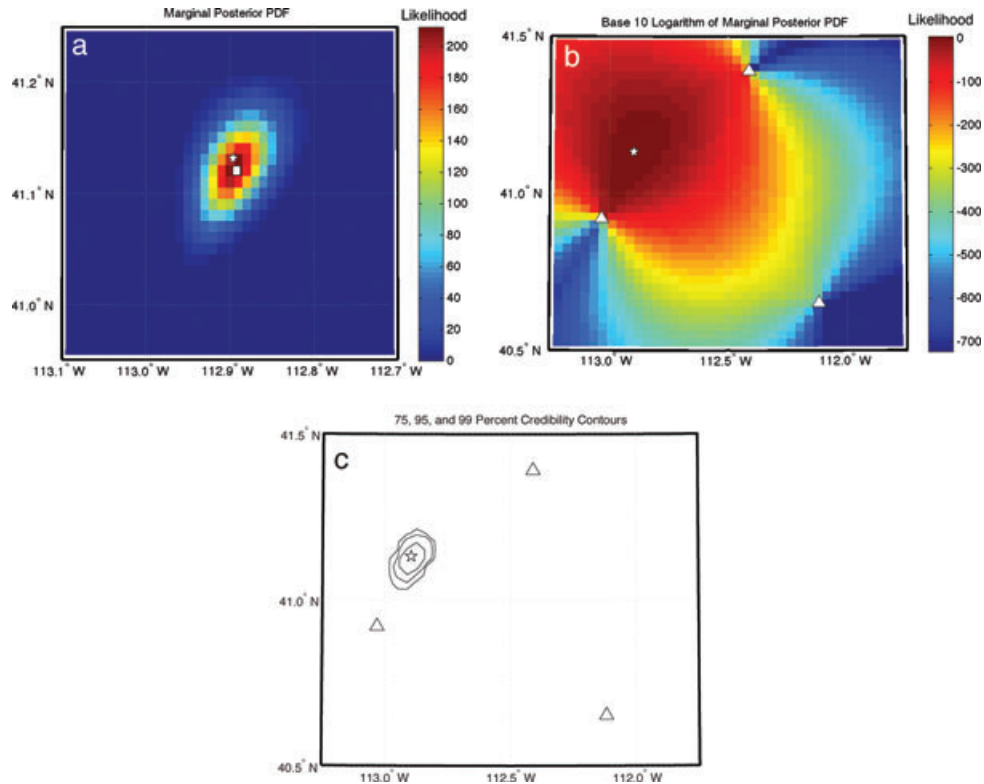


**Figure 3.** Location estimate obtained for the UTTR ground-truth event. Panels (a) and (b) show the marginal posterior PDF, and panel (c) shows the resulting credibility contours. Ground truth location is plotted in all panels as a white star, and the posterior mode source location estimate is plotted in panel (a) as a white rectangle.

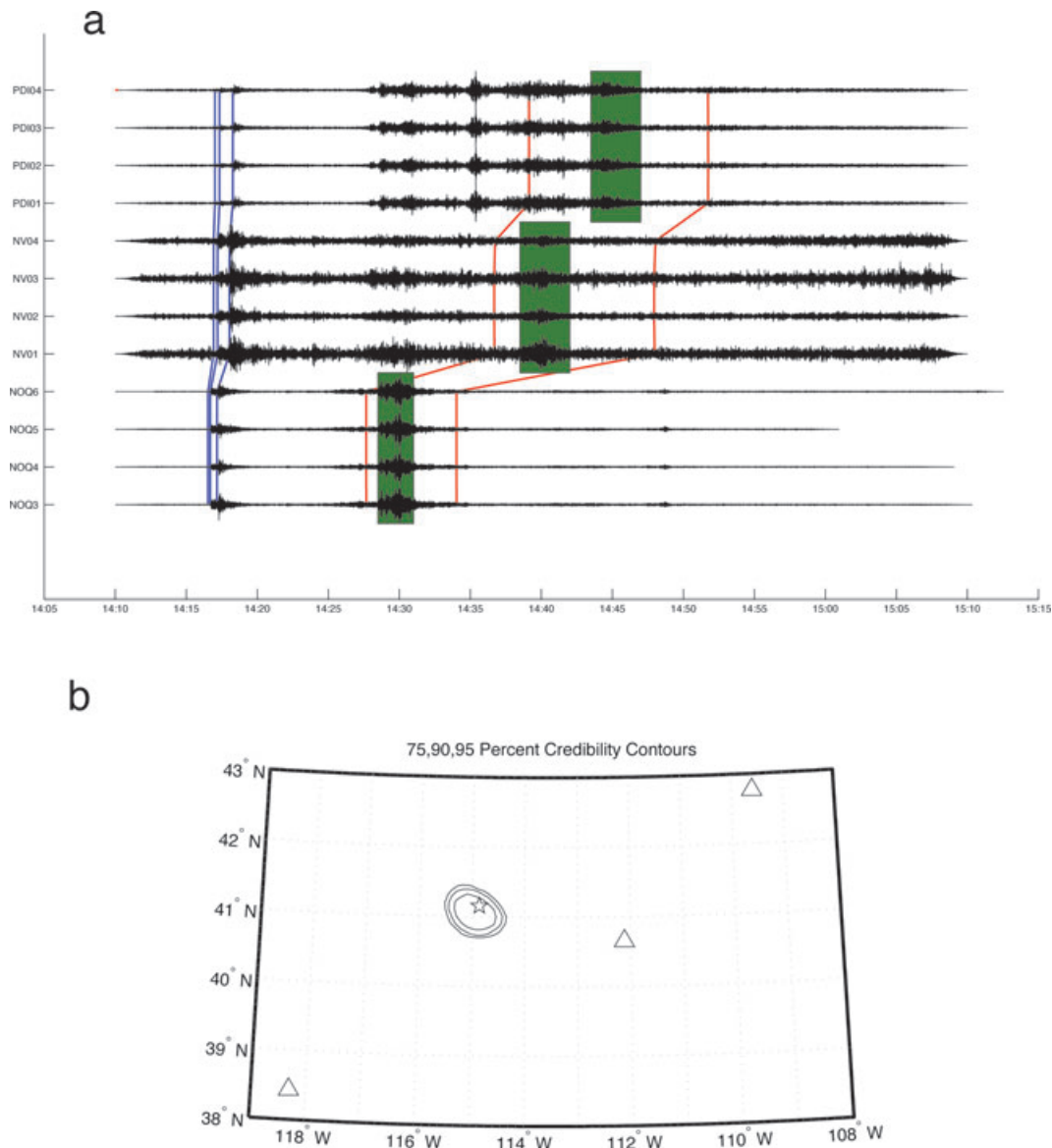


**Figure 4.** Results from applying the algorithm to infrasonic observations of the 2008 Wells, Nevada earthquake. Panel (a): Infrasonic observations at each array, where the green boxes highlight the arrivals used in estimating source location, blue lines represent predicted arrival times of seismic phases ( $P_n$ ,  $P_g$  and  $L_g$ ), and red lines denote the earliest and latest possible arrival times of epicentral infrasound arrivals. Panel (b): 75, 90 and 95 per cent credibility contours obtained from the algorithm. The seismically-derived location solution is shown by a star (associated seismic localization uncertainties and the BISL posterior mode are not depicted).

Figs 1 and 2, we observed similar relative orientations of arrival time and backazimuth contours for the other simulated events. The phenomenon appears somewhat simpler when the arrays lie in a collinear configuration. In this case, the arrival time contours tend to run perpendicular to the arrays, while the backazimuth contours tend to run parallel to the arrays.

Another conspicuous feature of the BISL algorithm concerns the rapid drop in the marginal posterior PDF away from the central peak. As shown by plotting its logarithm in Fig. 2, the marginal posterior PDF undergoes a drop of many orders of magnitude away from the source location estimate. This rapid rate of decay arises from the statistical assumptions encoded in the likelihood function and may be justified if large errors are uncommon. If, on the other hand, data outliers are not uncommon, revision of the probability model might prove useful. Finally, comparison of the logarithms of  $\Theta$  and  $\Phi$  in Fig. 1 shows that the backazimuth function drops

off more quickly than the arrival time function. Given the greater discriminating power traditionally attributed to backazimuths over arrival times, it seems appropriate that the backazimuth function exerts a stronger influence through its faster rate of decay.

Determination and calibration of the variance components  $\sigma_{\theta, \text{meas}}^2$ ,  $\sigma_{\theta, \text{mod}}^2$ ,  $\sigma_{\phi, \text{meas}}^2$  and  $\sigma_{\phi, \text{mod}}^2$  can be accomplished through appropriate experimentation or analysis of ground-truth events. A random effects linear model can be used to analyse these data and decompose the total variability into component sources of error. Development of these methods are key to the implementation of BISL.

An alternative arrival time formulation currently being pursued involves changing the underlying way in which the arrival time model error is incorporated within the likelihood function. Following the original formulation, the observed arrival time equals the sum of the origin time, traveltime, and measurement and model

error:

$$t_i = t_0 + \frac{d_i}{v} + \epsilon_{\text{meas}} + \epsilon_{\text{mod}}. \quad (11)$$

A significant advantage of this representation is that the error terms  $\epsilon_{\text{meas}}$  and  $\epsilon_{\text{mod}}$  are additive. Treating model error differently, eq. (11) might be rewritten

$$t_i = t_0 + \frac{d_i}{v + \epsilon(v, \sigma)} + \epsilon_{\text{meas}}, \quad (12)$$

where some statistical distribution of group velocity variations  $\epsilon(v, \sigma)$  about the parameter  $v$ , representing the average group velocity, is assumed. Though the mathematical implications are more complex, eq. (12) provides a more satisfying treatment of the arrival time model error and a possible topic for future investigation.

## CONCLUSIONS

Building on Arrowsmith *et al.* (2008), we have developed a Bayesian statistical framework for locating infrasound events that combines arrival times and backazimuths in the source location analysis. The method accounts for uncertainty in path and phase identification by placing a prior PDF on infrasonic group velocity. This prior folds model error into source location estimation and the determination of the associated Bayesian credibility regions. We have demonstrated the method using synthetic data (without noise) and two ground truth events. Although the ground-truth examples in this paper assume no phase identification, the group velocity range in eq. (2) can be modified accordingly if phases can be reliably identified. In many cases, however, it is difficult to robustly identify phase due to the possibility of overlapping arrival time ranges and present limitations in capturing and incorporating atmospheric properties. The framework presented in this paper provides one approach for overcoming this difficulty.

## ACKNOWLEDGMENTS

We thank Prof Jeannot Trampert and two anonymous reviewers for their constructive comments on an earlier version of this manuscript. The authors acknowledge the support of Ms Leslie A. Casey and the National Nuclear Security Administration Office of Nonproliferation Research and Development for funding this work. This work was completed under the auspices of the U.S. Department of Energy by Los Alamos National Laboratory under contract DE-AC52-06NA24596.

## REFERENCES

- Arrowsmith, S.J., Drob, D., Hedlin, M.A.H. & Edwards, W., 2007. A joint seismic and acoustic study of the Washington State bolide, *J. geophys. Res.*, **112**, doi:10.1029/2006JD008001.
- Arrowsmith, S.J. *et al.*, 2008. Regional monitoring of infrasound events using multiple arrays: application to Utah and Washington State, *Geophys. J. Int.*, **175**, 291–300. doi:10.1111/j.1365-246X.2008.03912.x.
- Arrowsmith, S.J., Burlacu, R., Whitaker, R. & Randall, G., 2009. A repeating secondary source of infrasound from the Wells, Nevada, earthquake sequence, *Geophys. Res. Lett.*, **36**, doi:10.1029/2009GL038363.
- Berger, J.O., 1985. *Statistical Decision Theory and Bayesian Analysis*, 2nd edn., Chapman & Hall, New York.
- Bernardo, J.M. & Smith, A.F.M., 2000. *Bayesian Theory*, John Wiley & Sons, Inc., New York.
- Ceplecha, Z., Borovicka, J., Elford, W.G., ReVelle, D.O., Hawkes, R.L., Porubcan, V. & Simel, M., 1998. Meteor phenomena and bodies, *Space Sci. Rev.*, **84**, 327–471.
- Ceranna, L., Le Pichon, A., Green, D.N. & Mialle, P., 2009. The Buncefield explosion: a benchmark for infrasound analysis across Central Europe, *Geophys. J. Int.*, **177**, 491–508.
- Drob, D., 2004. Atmospheric specifications for infrasound calculations, *Infrasound*, **5**, 6–13.
- Evers, L.G., Ceranna, L., Haak, H.W., Le Pichon, A. & Whitaker, R.W., 2007. The Buncefield explosion; a benchmark for infrasound analysis across Central Europe, *Bull. seism. Soc. Am.*, **97**, 417–425.
- Fagan, D.K., Taylor, S.R., Schult, F.R. & Anderson, D.N., 2009. Using ancillary information to improve hypocenter estimation: Bayesian single event location (BSEL), *Pure appl. Geophys.*, **166**, 521–545.
- Garces, M., Hansen, R.A. & Lindquist, K.G., 1998. Traveltimes for infrasonic waves propagating in a stratified atmosphere, *Geophys. J. Int.*, **135**, 255–263.
- Garces, M., Drob, D.P. & Picone, J.M., 2002. A theoretical study of the effect of geomagnetic fluctuations and solar tides on the propagation of infrasonic waves in the upper atmosphere, *Geophys. J. Int.*, **148**, 77–87.
- Le Pichon, A., Vergoz, J., Herry, P. & Ceranna, L., 2008. Analyzing the detection capability of infrasound arrays in central Europe, *J. geophys. Res.*, **113**, doi:10.1029/2007JD009509.
- Mutschlechner, J.P. & Whitaker, R.W., 2005. Infrasound from earthquakes, *J. geophys. Res.*, **110**, doi:10.1029/2004JD005067.
- Seber, G.A.F. & Wild, C.J., 1989. *Nonlinear Regression*, John Wiley & Sons, New York.
- Stump, B., Jun, M.-S., Hayward, C., Jeon, J.-S., Che, I.-Y., Thomason, K., House, S.M. & McKenna, J., 2004. Small-aperture seismo-acoustic arrays: design, implementation, and utilization, *Bull. seism. Soc. Am.*, **94**, 220–236.
- Stump, B.W. *et al.*, 2008. Shear velocity structure in NE China and characterization of infrasound wave propagation in the 1-210 kilometer range, *Proc. 2008 Monitoring Res. Rev.*, pp. 287–296.
- Szuberla, C.A.L. & Olson, J.V., 2004. Uncertainties associated with parameter estimation in atmospheric infrasound arrays, *J. acoust. Soc. Am.*, **115**, 253–258.